Energy Equip. Sys./ Vol. 13/No. 2/June 2025/ 169-191

ENERGY EQUIPSYS

Energy Equipment and Systems

www.energyequipsys.com

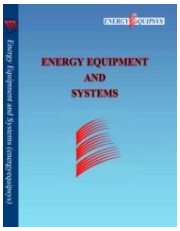

A comprehensive experimental approach to understanding the effects of surface wettability on bubble formation at submerged orifices

Authors

Sara Izadiamoli[a]
Mohsen Mashhadi Kashtiban[b]
Amirmohammad Sattari[c*]
Pedram Hanafizadeh[b]

[a] Department of Mechanical and Aerospace Engineering, Politecnico di Torino, Torino 10129, Italy.

[b] School of Mechanical Engineering, College of Engineering, University of Tehran, Tehran, Iran.

[c] Department of Mechanical Engineering, K. N. Toosi University of Technology, Tehran, Iran.

Article history:
Received: 6 October 2024
Revised: 14 November 2024
Accepted : 22 November 2024

ABSTRACT

This research investigates single-bubble growth through experimental gas injection into submerged orifices immersed in distilled water at room temperature. The study examines various parameters that effect bubble dynamics, including orifice diameter (1, 2, and 3 mm), surface wettability (neutral aluminum, hydrophilic, superhydrophobic), and gas injection flow rate (12-60 mlph). Bubbles are generated via air injection into the liquid column using a syringe pump, and bubble formation characteristics are analyzed using image processing techniques and the Young-Laplace equation. Force analysis is employed to evaluate the results further. The study identifies three distinct stages in bubble growth: waiting, expansion, and necking. Decreasing the wettability of the orifice leads to an increase in both the volume and Reynolds number of the separation bubble while reducing the frequency of bubble growth. Notably, bubbles formed at superhydrophobic orifices exhibit unique characteristics. For example, necking of the bubble occurs rapidly due to the contact angle never reaching 90°, resulting in a significant velocity increase during detachment. Additionally, the contact line of the bubble remains in a steady state condition throughout its growth.

Keywords: Bubble Formation; Surface Wettability; Force Analysis; Hydrophilic; Superhydrophobic.

1. Introduction

The understanding of bubbly flows and bubble dynamics holds paramount importance across a spectrum of industries, including nuclear power plants, boilers, heat converters, petrochemicals, bioreactors, aerospace, pharmacy, agriculture, water refineries, and beyond [1–3]. In bubbly flows, the interplay of various forces leads to the formation of numerous curved intersections, culminating in the creation of spherical bubbles.

Previous theoretical and empirical studies have investigated bubble growth through various approaches, including analyzing changes in the contact angle on surfaces and considering the balance of influential forces acting on the bubble during its evolution. These studies have proposed various step-wise models for bubble growth, including one-step, two-step, three-step, and four-step processes [4–6]. For example, Gnyloskurenko et al. [7] conducted a study on bubble formation using the force balance method and found that the growth of

* Corresponding author: Amirmohammad Sattari
School of Mechanical Engineering, College of Engineering, University of Tehran, Tehran, Iran
Email: amirmsattari@kntu.ac.ir

bubbles is mainly influenced by the hysteresis contact angle. They identified four stages of bubble growth: nucleation, under-critical growth, critical growth, and necking. In another study, Di Bari and Robinson (2013) observed the growth of bubbles in three steps by investigating changes in the contact angle of bubbles on orifices with different surface wettabilities [5]. In the initial step, the contact angle of the bubbles gradually decreases. Subsequently, in the second step, as the bubble's volume expands, the upper section experiences the influence of buoyancy forces, inducing alterations in both the contact angle and the rate of center of mass. Finally, in the third step, the buoyancy force in the upper section further intensifies, causing the stretching of the bubble's tip and the onset of necking, which in turn leads to an increase in the contact angle.

Studies indicate that the dynamics of bubbles are influenced by various factors, encompassing the volumetric flow rate of gas injected into the nozzles, wettability, size, and shape of the nozzles, volume of the water chamber, liquid column height, and physical properties of both the liquid and gas phases. Here, we will briefly outline some of the most significant factors.

1.1. Wettability

The contact angle of the nozzle surface plays a pivotal role in influencing bubble dynamics and formation frequency, representing the wettability or surface energy of the nozzle. Marmur and Rubin [8] showcased that in superhydrophilic orifices, the radius of the bubble's contact line remains consistent throughout its development. Conversely, in neutral and superhydrophobic orifices, the radius exceeds the inner diameter of the orifice at each stage of evolution.

Gnyloskurenko et al. [9] conducted a study investigating the influence of surface contact angle on bubble formation. They classified orifice surfaces into three categories: hydrophilic, neutral, and hydrophobic. The researchers discovered that as the wettability of the orifice surface increased, the volume and duration of separated bubbles decreased, and the shape of the bubbles tended towards spherical. Additionally, they noted that bubbles formed along the edges of the inner diameter of hydrophilic orifices, while on hydrophobic orifices, the contact line of bubbles spread widely across the surface, extending beyond the inner diameter.

Kasimsetty et al. [10] performed both experimental and numerical investigations into bubble growth stemming from air injection into a submerged orifice. Their findings revealed that the radius of the bubble's contact line remained fixed along the edges of the inner diameter of a hydrophilic orifice, while it exceeded the edges in hydrophobic and neutral orifices. In a separate study, Cai et al. [11] delved into the behavior of bubbles within a viscous liquid. They concluded that reducing the wettability of the orifice surface augmented the surface tension force, consequently leading to a larger separation volume.

Abbassi et al. [12] investigated bubble formation from orifices with varying surface contact angles (60°, 90°, and 120°). Their study revealed that as the surface contact angle of the orifice increased (indicating reduced wettability), the diameter of the bubble's contact line also increased. This expansion in diameter corresponded to an augmentation in the surface tension force and the volume of the bubble. Furthermore, the research noted that decreasing the surface wettability led to an increase in the width of the neck formed during bubble formation.

1.2. Volumetric flow rate

The volumetric flow rate of gas injection plays a pivotal role in the examination of bubble dynamics and its influence on bubble growth and the nature of two-phase flow. This flow rate impacts various stages of bubble evolution, encompassing the initial nonlinear progression of bubble volume, neck expansion subsequent to coalescence, and post-coalescence oscillation [13]. Moreover, it affects bubble generation, detachment time, and dynamics, along with the pressure field surrounding the bubbles post-detachment [14,15]. Furthermore, the gas injection method, including factors such as radial positioning, the number of gas nozzles, and their spacing, can alter the flow structure in viscous liquids [16]. Together with other variables such as initial bubble diameter, liquid viscosity, and surface tension, the volumetric

flow rate of gas injection determines bubble deformation and the internal flow field within the bubble [17].

According to Kasimsetty et al. [10], an increase in gas flow rate diminishes the impact of surface contact angle and orifice diameter on bubble formation, while amplifying the dependency of bubble volume on flow rate. This effect on bubble volume is less pronounced in nozzles with high and neutral wettability but more significant in nozzles with poor wettability, as noted by Corchero et al. [18]. Vafaei and Wen conducted empirical investigations on bubble formation utilizing submerged micrometer-sized nozzles, as well as submerged stainless steel substrate and needle nozzles [19,20]. They observed that at lower flow rates, bubble formation occurs quasi-statically, with a balance between upward and downward forces. As the separation moment of bubbles approaches, the influence of buoyancy force increases, leading to upward elongation of the bubbles and greater consideration of liquid viscosity. Additionally, bubble characteristics such as immediate contact angle, apex radius, contact line radius, and height are predominantly influenced by the volume of the bubble and weakly affected by gas flow rate. Gerlach et al. [21] investigated the quasi-static formation of bubbles from submerged orifices and determined that the gas flow rate through the orifices minimally impacts pressure variations, and the viscous tension of the gas-liquid interface can be disregarded.

1.3. Orifice size

Previous experimental and numerical investigations consistently indicate that increasing the internal diameter of nozzles yields larger bubble volumes but lower bubble frequencies (20,22). Gerlach et al. [21] delved into the formation of air bubbles through brass and Teflon-submerged orifices with radii of 0.5 mm, 1 mm, and 2 mm. They explored the effects of gas pressure, surface tension, hydrostatic pressure, and ambient pressure on bubble formation. Their findings corroborate the assertion by Di Bari and Robinson [5] that surface tension force plays a crucial role in the formation of small bubbles in orifices with small radii. They investigated adiabatic gas bubbles across flow rates of 10-100 mlph and noted that the forces involved vary with orifice size. Smaller orifices produce smaller bubbles, leading to a reduction in buoyancy force. Additionally, they observed a direct correlation between the contact pressure force during separation and the orifice diameter. Orifice diameter size also influences bubble development and separation. Smaller orifices facilitate faster detachment and the formation of more spherical-shaped bubbles, while larger orifices result in larger volume bubbles and longer formation times.

Tariqul Islam et al. [23] conducted a study on the impact of different orifice sizes (ranging from 0.5-1.5 mm) on bubble characteristics under a gas inlet velocity of 0.2 m/s. They found that smaller orifices led to smaller bubbles and quicker formation of a hemispherical shape. Abbassi et al. [24] investigated the bubble formation process from orifices with diameters of 1 and 2 mm. They concluded that, at constant flow rates, larger orifices generated larger bubbles within a similar timeframe. This is attributed to an increase in bubble diameter resulting in more air injected into the orifice, thereby increasing the width and height of the bubble neck. Additionally, the larger orifice's greater contact line results in a higher surface tension force.

1.4. Novelty of the work

While previous studies have explored the influence of surface wettability on bubble formation, this research offers a comprehensive experimental approach that investigates the phenomenon across multiple orifice diameters (1, 2, and 3 mm) and wettability conditions (neutral aluminum, hydrophilic, and superhydrophobic). This detailed examination goes beyond past research by not only analyzing bubble formation time and volume but also revealing distinct bubble behavior on superhydrophobic surfaces, including a constant contact line, diminished influence of diameter on growth, and a stronger dependence on flow rates for normalized bubble volume. Additionally, the study highlights the significance of the drag force specifically for superhydrophobic orifices, a factor often neglected in conventional studies. By

examining a broad spectrum of surface wettability and orifice sizes, the research uniquely captures how these factors interact to shape bubble dynamics, offering insights that were previously unexplored. This work also introduces a nuanced understanding of bubble detachment, particularly by quantifying how drag influences this process on superhydrophobic surfaces, which is essential for applications demanding precise bubble size and controlled detachment. Furthermore, the discovery that superhydrophobic surfaces exhibit a stable contact line behavior provides new perspectives for microfluidic applications, where consistent interface properties are crucial for device reliability. These contributions suggest a potential advancement in the understanding of bubble formation dynamics, highlighting implications for improved fluid manipulation techniques and enhanced predictability in applications ranging from biomedical devices to chemical processing.

Nomenclature

a_{CM}	Acceleration central of mass acceleration (m/s^2)
C_D	Drag coefficient
D	Inner diameter of orifice (m)
D_{eq}	Equivalent diameter of the bubble (m)
f	Frequency of bubble formation (Hz)
F_B	Buoyancy force (N)
F_D	Dynamic force (N)
F_P	Pressure force (N)
F_γ	Surface tension force (N)
g	Acceleration of gravity (m/s^2)
H	Height of the bubble (m)
m_g	Mass of bubble (kg)
P_0	Air pressure (Pa)
P_g	Inner pressure of bubble (gas pressure) (Pa)
P_l	liquid column pressure (Pa)
Q	Injecting gas flow rate (m^3/s)
R_1	Radiuses of the main curvature (m)
R_2	Radiuses of the main curvature (m)
R_o	Radius curvature at the tip of the bubble (m)
Re	Reynolds number
r	Horizontal vector (m)
r_d	Radius of the contact line of the bubble (m)
r_d	Radius of the contact line of the bubble (m)
S	Curvature of bubble (m)
t	Time (sec)
U_g	Superficial velocity (m/s)
u_{CM}	Velocity of the central mass (m/s)
V	Bubble volume (m^3)
V_m	Volume of bubble from the top of neck (m^3)
W_{max}	Maximum width of bubble (m)
Z	Vertical vector (m)

Greek symbols

γ	Surface tension of orifice (N/m)
δ	Height of the water column (m)
θ	Contact angle of the small element of the bubble
θ_0	Contact angle of bubble
μ_d	Viscosity of bubble (Pa.s)
ρ_g	Density of air (kg/m^3)
ρ_l	Density of water (kg/m^3)

Subscripts

g	Gas
l	Liquid
lg	Liquid-gas

2. Methodology

2.1. Experimental apparatus

Figure 1 depicts the experimental setup designed to investigate bubble formation and separation. The setup comprises a syringe pump, high-speed camera, water container, air-injecting orifices, and LED lamp. The bubble column is a PMMA cube with a 120×120 mm² cross-section and 300 mm height. The open top exposes the column to atmospheric pressure. The water level is fixed at 50 mm from the orifice tip, as liquid column height minimally affects bubble dynamics. Air injection occurs under a constant volumetric flow rate using an automatic syringe pump (1% accuracy) capable of maintaining both steady flow and high pressure (approximately 2 bars). A high-speed camera (1000 fps, 1728×768 pixels) captures bubble movement. Image processing code written in Matlab software analyzes the bubble border and characteristics like volume, height, frequency, and contact angle. An LED lamp further enhances the image quality of the camera.

A combination of acid etching and thermal treatment was used to create both hydrophilic and superhydrophobic surfaces. By immersing the orifices in 37% HCl and 35% H_2O_2, followed by heating at 600°C for 4 hours, a hydrophilic surface with a contact angle of 16.035° was achieved. For the superhydrophobic surface, a coating of 97%

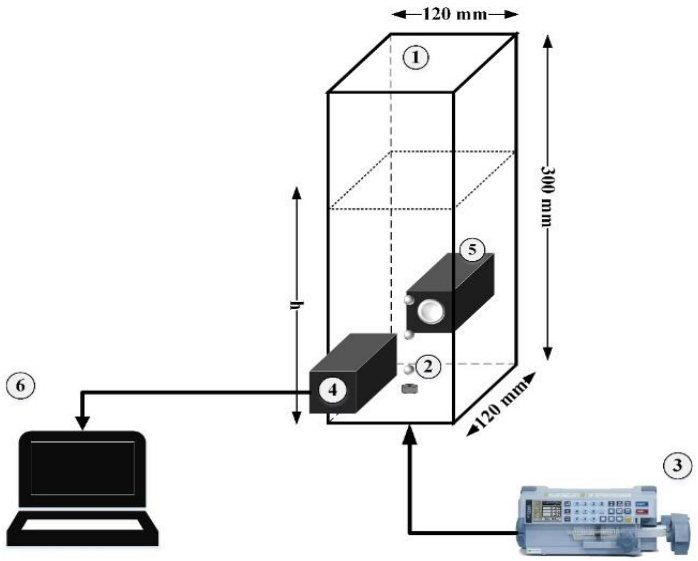

Fig. 1. The schematic view of the experimental apparatus includes the following components: (1) liquid column, (2) orifice, (3) syringe pump, (4) high-speed camera, (5) LED lamp, and (6) computer.

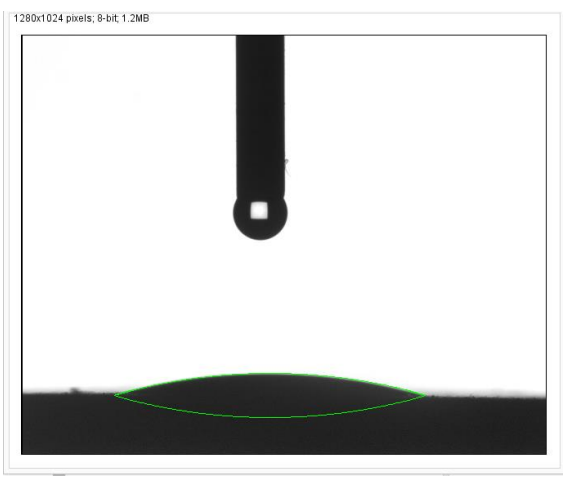

(a)

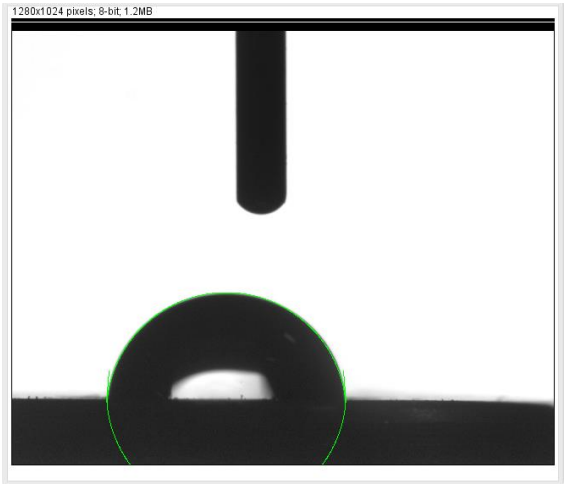

(b)

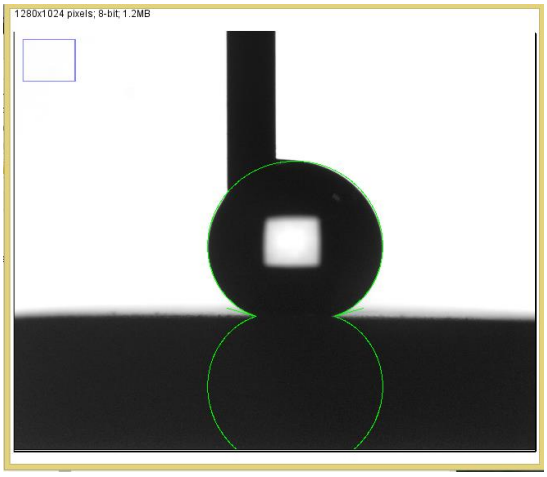

(c)

Fig. 2. Results of contact angle measurement for: (a) hydrophilic, (b) neutral, and (c) superhydrophobic surfaces.

FAS-17 was applied after the etching process, followed by heating at 200°C for 2 hours. This resulted in a contact angle of 163.344°, indicating a highly water-repellent surface. The contact angle of the neutral aluminum was determined to be 85.338°. The wettability of the orifice plates is evaluated using a contact angle goniometer device (Jikan CAG-20SE), and the resulting figures are shown in Fig. 2 This significant difference in contact angles demonstrates the effectiveness of the chosen approach. Further studies could explore the long-term stability of these surfaces and their performance under different operating conditions.

This study utilized orifices with a height of 20 mm and an external diameter of 10 mm, as detailed in Fig. 3. Internal diameters of 1 mm, 2 mm, and 3 mm were chosen for analysis. To explore the influence of flow rate on the observed phenomena, experiments were conducted across a range of flow rates, varying from 12 to 60 ml/h. Table 1 summarizes the key parameters employed in this study.

To minimize experimental error and its influence on results, each experiment was repeated at least three times, thereby controlling for random fluctuations and potential user error. The accuracy of the experiments is quantified in Table 2, indicating the uncertainty based on the precision of the instruments used. This uncertainty is further visualized by the error bars in the figures, calculated as standard deviation.

Table 1. Range of operating conditions

Operating parameter	Parameter value
Flow rate	12-60 mlph
Liquid height above the orifice	50 mm
Liquid viscosity	0.001 Pa•s
Air viscosity	0.00018 Pa•s
Surface tension	72.5×10^{-3} N.m^{-1}
Liquid density	997.05 kg•m^{-3}
Air density	1.15 kg•m^{-3}
Orifice diameter	1-3 mm
Aluminum contact angle	85.3°±0.1
hydrophilic contact angle	16.0°±0.1
Superhydrophobic contact angle	163.3°±0.1

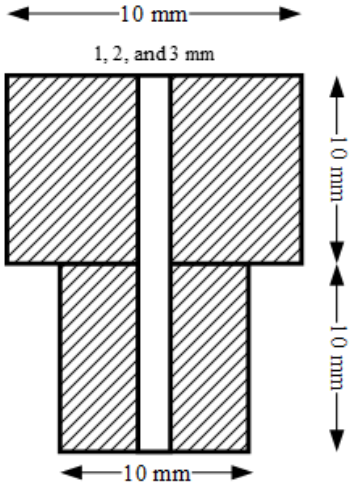

Fig. 3. Dimensions of the orifice plates

Table 2. Uncertainties in experimentally measured variables

Parameter	Amount of uncertainty	Uncertainty percentage
Air flow rate	–	1%
Image calibration scale	1 *pixel*	–

2.2. Image Processing Procedure

An image processing technique is used to extract bubble characteristics, employing preprocessing methods to minimize errors and utilizing Matlab R2020b for analysis. The process involves converting the original RGB images to grayscale and then to binary images to identify bubble edges. The bubble volume and dragged fluid volume are calculated by measuring the distance between the bubble center and its boundary, then rotating this element around the centerline to estimate the volume. The total bubble volume is aggregated from these sections, and the equivalent diameter is derived by assuming a sphere with the same volume. This method is also used to measure the volumes of the dragged and returning phases. Error bars indicate measurement errors, and the bubble characterizations were averaged over three trials, each analyzing about ten bubbles to ensure repeatability. For further details on the techniques, refer to Ref. [25].

2.3. Force balancing

The analysis of two-phase bubbly flows hinges critically on understanding the forces acting on bubbles during their evolution. To explore these dynamics, we adopt a quasi-equilibrium approach, simplifying the governing equations to a one-dimensional form. This simplification relies on the following assumptions:

- The experiments are conducted in room temperature (20 °C).
- The growth of the bubbles is adiabatic and axially symmetric.
- The properties of liquid and gas phases are considered to be constant.
- The liquid phase is stagnant.
- The gas pressure inside the bubble is uniform.

Figure 4 illustrates the forces acting on the system. Based on this analysis, the equilibrium force balance can be expressed mathematically as [5]

$$\sum \vec{F} = \overrightarrow{F_B} + \overrightarrow{F_P} + \overrightarrow{F_\gamma} + \overrightarrow{F_D} = 0 \qquad (1)$$

where $F_B . F_P . F_\gamma$ and F_D are the forces of buoyancy, pressure, surface tension, and dynamic forces, respectively.

At the outset of bubble growth, its small size allows surface tension to exert the dominant downward force, pinning it to the orifice surface. However, as the bubble expands and its volume increases, upward forces like buoyancy also intensify, outpacing the downward forces. This growing dominance of the upward vector forces eventually reaches a tipping point where their resultant becomes positive, leading the bubble to detach from the orifice surface.

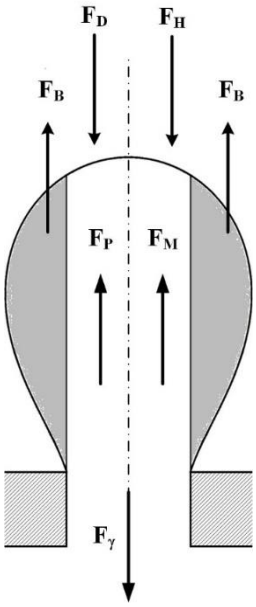

Fig. 4. Effective forces acting on a growing bubble

The buoyancy force (F_B) is the upward force exerted on a bubble due to the weight of the liquid it displaces. According to Archimedes' principle, the buoyancy force is equal to the weight of the displaced fluid. To calculate the buoyancy force, the hydrostatic components of liquid pressure on the apex of the bubble are integrated [5]. Thus,

$$F_B = \int \left(\rho_l - \rho_g\right) g dV = V_m \left(\rho_l - \rho_g\right) g \qquad (2)$$

where, V_m is the volume of the bubble from the top of the bubble neck. Therefore, the equivalent diameter of the bubble D_{eq} is calculated using

$$V_m = \pi \frac{D_{eq}^3}{6} \Rightarrow D_{eq} = \left(\frac{6V_m}{\pi}\right)^{\frac{1}{3}} \qquad (3)$$

The surface tension force (F_γ) is calculated using

$$F_\gamma = P\gamma sin\theta_o = 2\pi r_d \gamma sin\theta_o \qquad (4)$$

where P is the contact perimeter of the bottom of the bubble with the orifice, θ_o is the contact angle of the orifice surface and r_d is considered as the radius of the contact line of the bubble with the orifice. The role of surface tension force is so evident at low gas flow rates due to insignificant Reynolds number and drag force. According to Fig. 4, the pressure force (F_p) at the tip of the bubble is computed using

$$F_p(H) = \Delta P(H) \pi r_d^{\,2} = (P_g - P_l) \pi r_d^{\,2} = \left(\frac{2\gamma_{lg}}{R_0} - \left(\rho_l - \rho_g\right) gH\right) \pi r_d^{\,2} \qquad (5)$$

where P_g and P_l are the inner pressure of the bubble and the liquid column pressure on the tip of the bubble, and the hydrostatic force of the bubble (F_H) is written as $\left(\left(\rho_l - \rho_g\right) gH\right) \pi r_d^{\,2}$.

Following [26], the momentum force can be calculated as

$$F_{momentum} = m_g a_{CM} = \rho_g U_g Q \qquad (6)$$

where, m_g and a_{CM} are the mass and the central of mass acceleration of the bubble, respectively. ρ_g, U_g, and Q are the density, the superficial velocity ($U_g = 4Q/\pi D^2$), and the volumetric flow rate of the gas phase, respectively. However, according to Oguz and Prosperetti [27], it is important to consider that when the gas density is within a certain range and the injection gas flow rate is below the critical value, the momentum force of the gas can be disregarded and the bubble can be assumed to be in a quasi-static state.

Following [28], The drag force can be represented as

$$F_D = \frac{1}{2} \rho_l C_D u_{CM}^2 \frac{\pi W_{max}^{\,2}}{4} \qquad (7)$$

where, ρ_l, u_{CM} and W_{max} are the density, the central mass velocity and the maximum width of the bubble, respectively. According to the statements of Morrison and Salman et. al [29,30], at the low Re numbers of the bubble, the drag coefficient (C_D) is evaluated as

$$C_D = \frac{24}{Re^{0.65}} \qquad (8)$$

The bubble Re number is define as

$$Re = \frac{\left(\rho_l - \rho_g\right)\left(U_b\right) D_{eq}}{\mu_d} \qquad (9)$$

where μ_d and U_b are the viscosity and the superficial velocity of the bubble, respectively.

The duration of the bubble formation process is defined as the period of between the separation of the previous bubble and the next one. The dimensionless time, which represents the elapsed time (t) to the total time of bubble formation (t_f), is expressed as

$$t^* = \frac{t}{t_f} \qquad (10)$$

3. Results and Discussion

The process of bubble formation unfolds in three distinct stages: Waiting, Expansion, and Detachment. In the Waiting stage, characterized by the absence of any formed bubble, downward forces predominate, and a defined interval of time elapses between the separation of the previous bubble and the emergence of the next. The Expansion stage initiates with the formation of the bubble and persists until the bubble begins to necking. Throughout this phase, upward forces gradually surpass downward forces. Finally, the Detachment stage transpires once the bubble necking has narrowed and is on the brink of separation. Here, upward forces entirely outmatch downward forces, propelling the bubble to accelerate upward [31].

Figure 5 illustrates the sequence of bubble formation for orifices with different wettability (hydrophilic, neutral, and superhydrophobic aluminum) having a diameter of 1 mm and a flow rate of 48 ml/h. The study examines the formation and growth of bubbles on various types of aluminum surfaces. On hydrophilic and neutral aluminum surfaces, bubbles initially form from the inner diameter of the orifice and undergo changes as they grow. Conversely, on superhydrophobic surfaces, bubbles originate from the outer diameter of the orifice and maintain a constant diameter until near separation. During separation, the buoyancy force experiences a significant increase, causing the bubble's contact line to decrease in diameter and detach from the surface. In hydrophilic and neutral aluminum orifices, the waiting stage accounts for more than 90% of the bubble formation duration. Utilizing hydrophilic and superhydrophobic orifices reduces the waiting stage of bubble formation. It is evident that decreasing the surface energy of the orifice (increasing hydrophobicity) prolongs the total time, volume, and height of the bubble formation process.

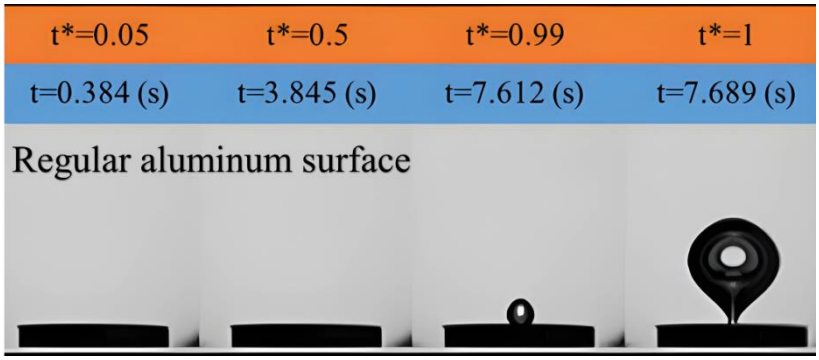

(a)

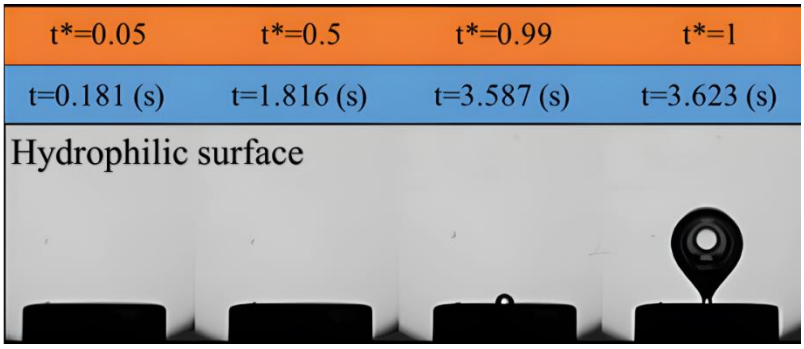

(b)

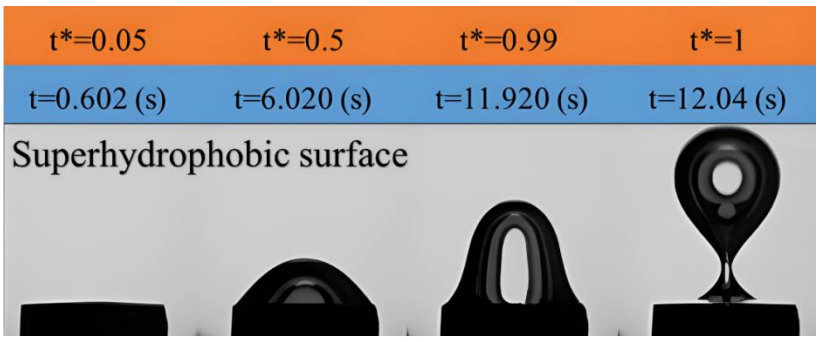

(c)

Fig. 5. Sequence of bubble formation in (a) neutral aluminum, (b) hydrophilic, and (c) superhydrophobic orifices

The growth rate of the bubble is dictated by the equilibrium between upward and downward forces. Figure 6 depicts the formation time of the bubble as a function of the flow rate for various orifice diameters and surface wettability conditions. The volume of the detached bubble and the frequency of bubble formation exhibit an inverse relationship. Increasing the diameter of the aluminum orifice from 1 to 3 mm reduces the formation time of the bubble, indicating an escalation in the growth rate (Fig.6 a, b, c). On a hydrophilic surface, the formation time of the bubble remains relatively constant as the orifice diameter increases from 1 to 2 mm. However, it increases when the diameter reaches 3 mm, resulting in a decline in the bubble growth rate (Fig.6a, b, c). Conversely, on a superhydrophobic surface, the volume of the bubble is relatively independent of the orifice size. Additionally, the dependence of the bubble formation time on the orifice size becomes negligible, especially at higher flow rates (Fig.6d).

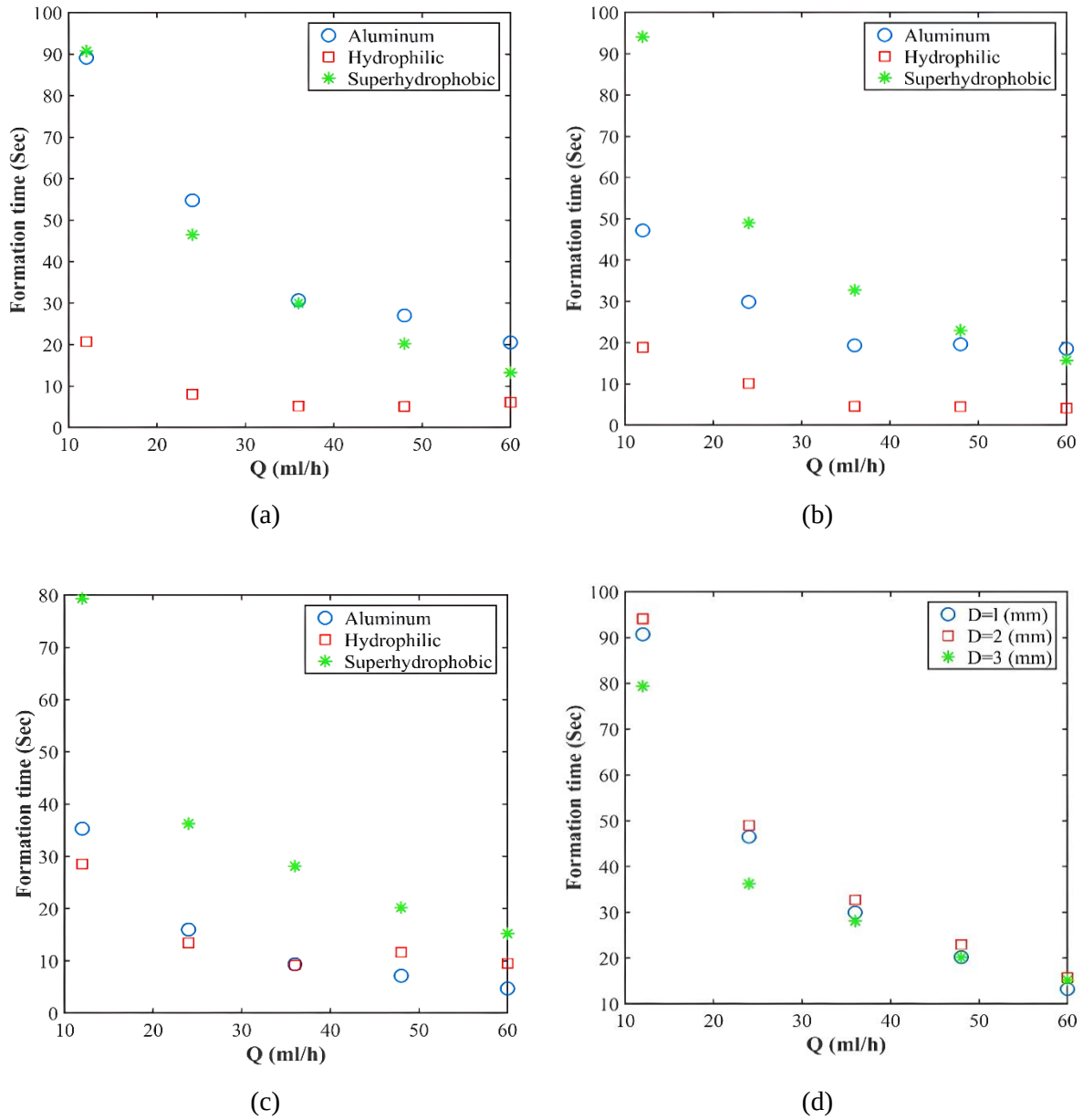

Fig. 6. Variation of the bubble formation time according to flow rates in orifice with diameter of a) 1 mm b) 2 mm, and c) 3 mm in different surface contact angles and in d) superhydrophobic orifice with different diameters

The diameter of the contact line of a bubble with an orifice remains unchanged or experiences a sharp drop during the necking stage [19,32]. Increasing the diameter of the orifice from 1 to 2 mm in neutral aluminum and hydrophilic orifices leads to a decrease in the contact angle at the separation moment of the bubble and its contact line diameter (Fig. 7). Additionally, increasing the diameter from 2 to 3 mm results in an increase in both bubble characteristics. However, on a superhydrophobic surface, the bubble contact line remains relatively constant and equal to the outer diameter of the orifice due to the greater impact of surface tension force with increased hydrophobicity (Fig. 7 a).

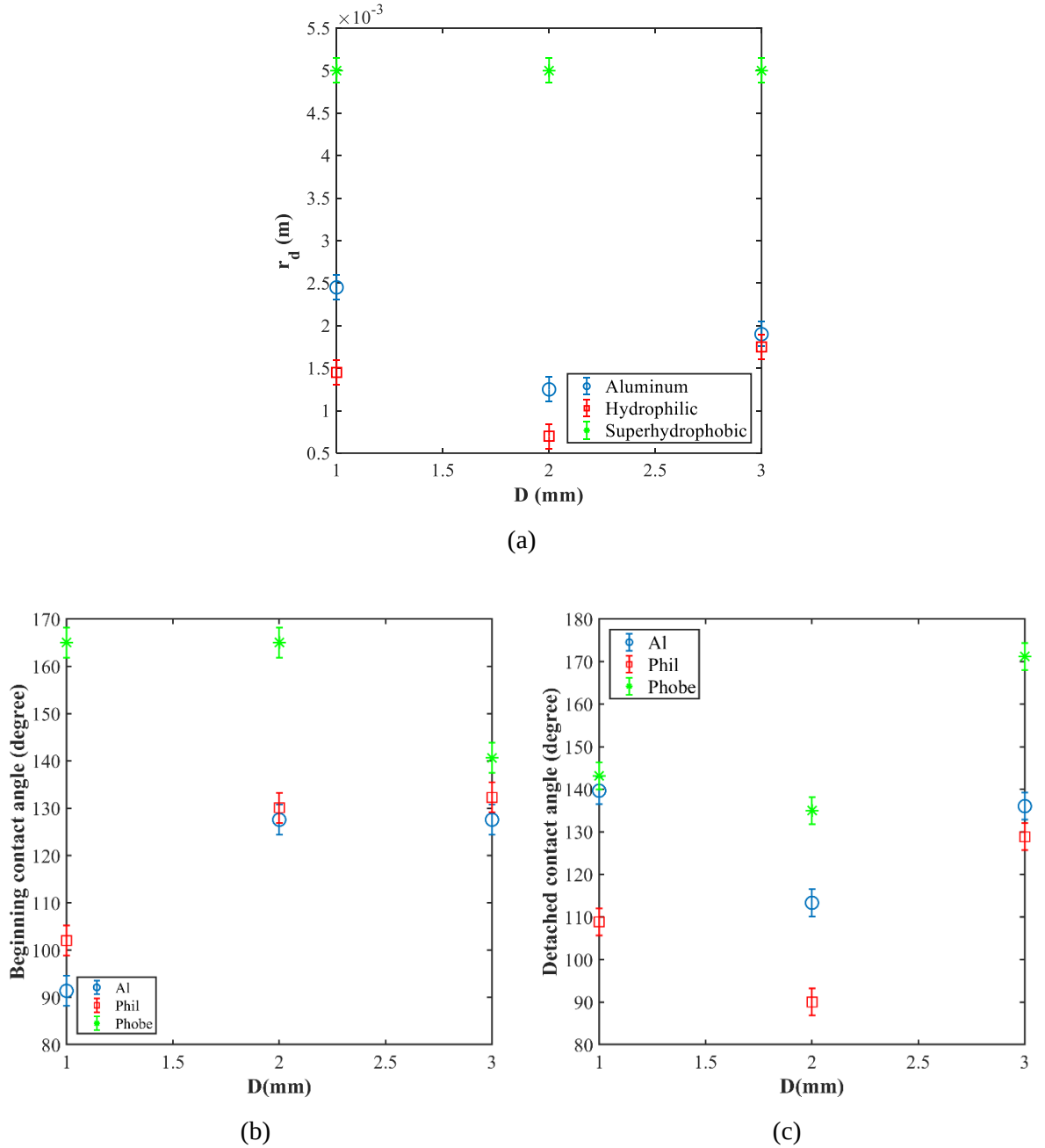

Fig. 7. (a) The size of diameter of bubble contact line in separation moment (b) contact angle of bubble beginning, and (c) separation contact angle of bubble on orifices with different diameters and contact angle surfaces under flow rate of 48 mlph.

Initially, the small volume of the bubble generates a considerable surface tension force, rendering the buoyancy force insignificant. However, as the bubble expands, the buoyancy force escalates while the contact angle progressively decreases until reaching a minimum value. Subsequently, upon reaching a critical threshold, the buoyancy force initiates an upward stretching of the bubble, leading to an increase in the contact angle until the separation moment. To analyze the fluctuation in bubble volume, we employ the normalized volume, represented by the ratio of the current bubble volume to the volume at the separation moment ($V^* = V/V_f$).

Figure 8 depicts the evolution of the normalized volume of a bubble over time in orifices with varying wettabilities. The plots reveal a progressive increase in the bubble's volume with time, signifying the growth rate of the bubble's expansion and eventual separation. During the separation phase, as the bubble nears detachment, there is a notable acceleration and velocity in bubble growth, resulting in a convergence of the expansion rates of bubble volume across different flow rates, particularly evident in larger orifices. Furthermore, enlarging the diameter of the orifice leads to a larger proportion of the bubble's expansion section compared to its weeping section. This observation suggests that in smaller orifices, the expansion section of the bubble is relatively smaller during formation, while the weeping section takes a longer time to develop.

The volume of the bubble at the separation moment is influenced by two key parameters: the duration of expansion and the expansion rate of the bubble. Figure 8c and Fig. 8f illustrate that increasing the diameter of the orifice from 1 mm to 2 mm leads to a reduction in both the expansion rate and the volume of the bubble at the separation moment. However, enlarging the diameter to 3 mm results in an increase in the volume of the detached bubble, while the expansion rate decreases. Figure 7a demonstrates that the volume of the separation bubble decreases when the orifice diameter increases from 1 to 2 mm but increases when the diameter increases to 3 mm. Figure 8c indicates that the normalized volume of the bubble increases with an increase in the orifice diameter in neutral aluminum at the same normalized time. Similarly, Fig. 8f shows that the normalized volume of the bubble increases when the orifice diameter increases from 1 to 2 mm but decreases when the diameter increases from 2 to 3 mm for the bubble generated from the hydrophilic orifice. This discrepancy is due to the decrease in the volume of the separation bubble when the orifice diameter increases from 1 mm to 2 mm and the subsequent increase in the volume of the separation bubble when the orifice diameter increases from 2 mm to 3 mm (Fig. 7b).

In at high flow rates, the influence of surface tension force diminishes, while upward forces assume a significant role. For a neutral aluminum orifice (Fig. 8a & b), augmenting the volumetric flow rate reduces the time needed to attain a specific bubble volume ratio. However, the expansion rate of the bubble diminishes with the increase in the bubble expansion section. In the case of a hydrophilic orifice with a diameter of 3 mm (Fig. 8d & e), elevating the volumetric flow rate from 36 to 60 mlph results in an escalation of the detached bubble volume and the velocity of the bubble's expansion section. This phenomenon occurs because more air enters the bubble, and the bubble spends less time in the expansion stage. The slopes of Fig. 8a & b suggest that as the diameter of the orifice increases in hydrophilic and neutral aluminum orifices, the dependence of the normalized bubble volume on the volumetric flow rate decreases. However, Fig. 8g & h illustrate that in the case of a superhydrophobic orifice with high surface tension force, alterations in flow rate and orifice size (Fig. 8I) exert minimal impact on the bubble volume, bubble genesis time, and the time required to reach a specific normalized volume.

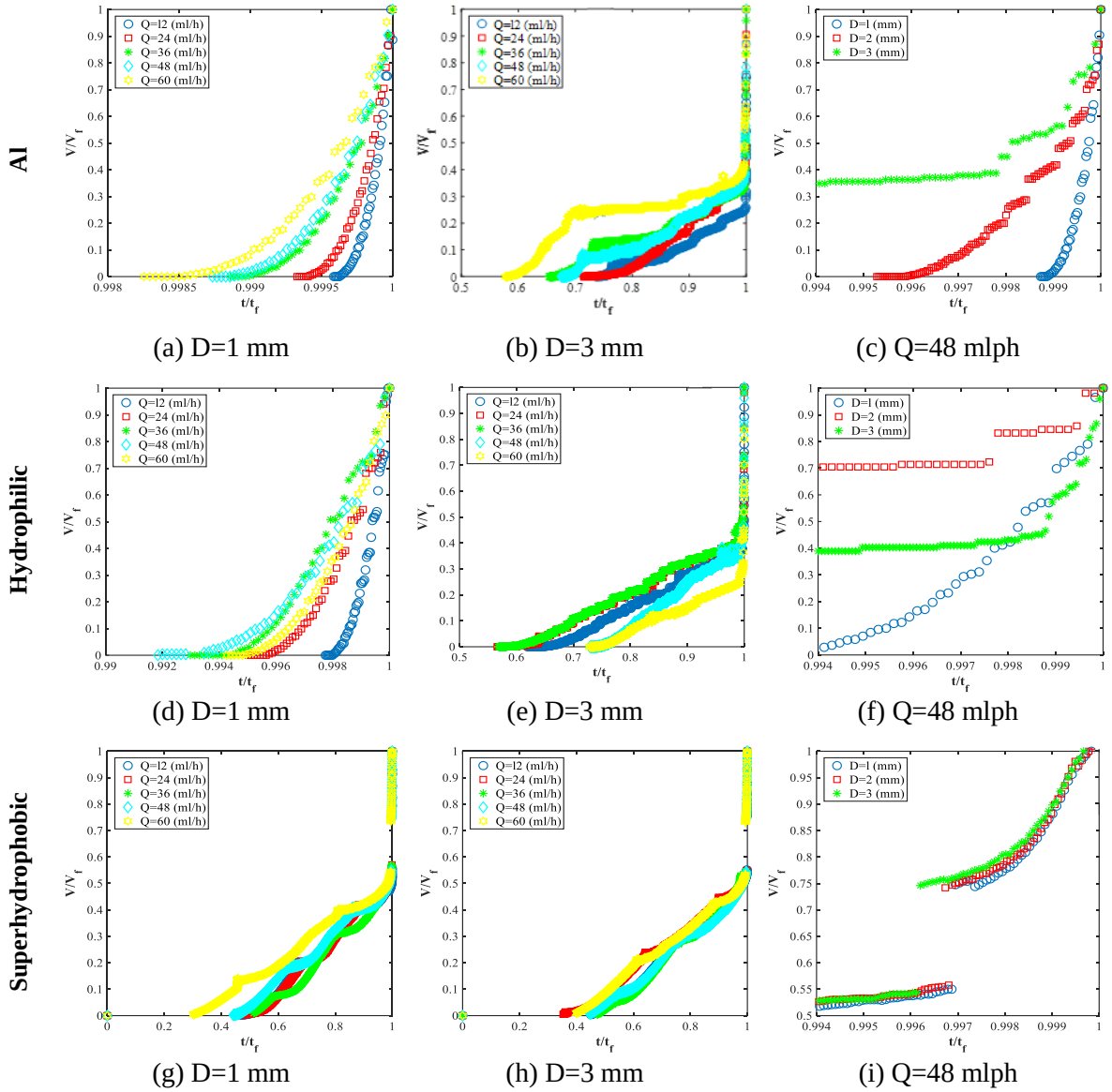

Fig. 8. The evolution of the normalized volume of the bubble over normalized time is investigated across three diameter orifices with distinct surface wettabilities: (a, b, c) neutral aluminum, (d, e, f) hydrophilic, and (g, h, i) superhydrophobic.

According to Kabanov et al.'s theory [33], the growth of bubble height and maximum width can elucidate the expansion and separation of a bubble into three stages. Initially, in the first stage, the bubble predominantly expands transversely, driven by the surface tension force prevailing over the buoyancy force. Subsequently, in the second stage, the bubble's volume primarily increases through its height, characterized by a subdued growth rate in height and nearly constant width growth. Finally, in the third stage, the buoyancy force asserts dominance, leading to accelerated growth in bubble height and detachment from the orifice.

The evolution of bubble height and width is depicted in Fig. 9. Both neutral and hydrophilic surfaces exhibit a similar trend, consistent with the aforementioned stages (Fig. 9a & b). On a superhydrophobic surface, the evolution of bubble height mirrors that of the other surfaces (Fig. 9c). However, the contact line diameter and maximum width of the bubble remain unchanged and steady until the necking stage, following which only the contact line diameter remains equal to the orifice diameter.

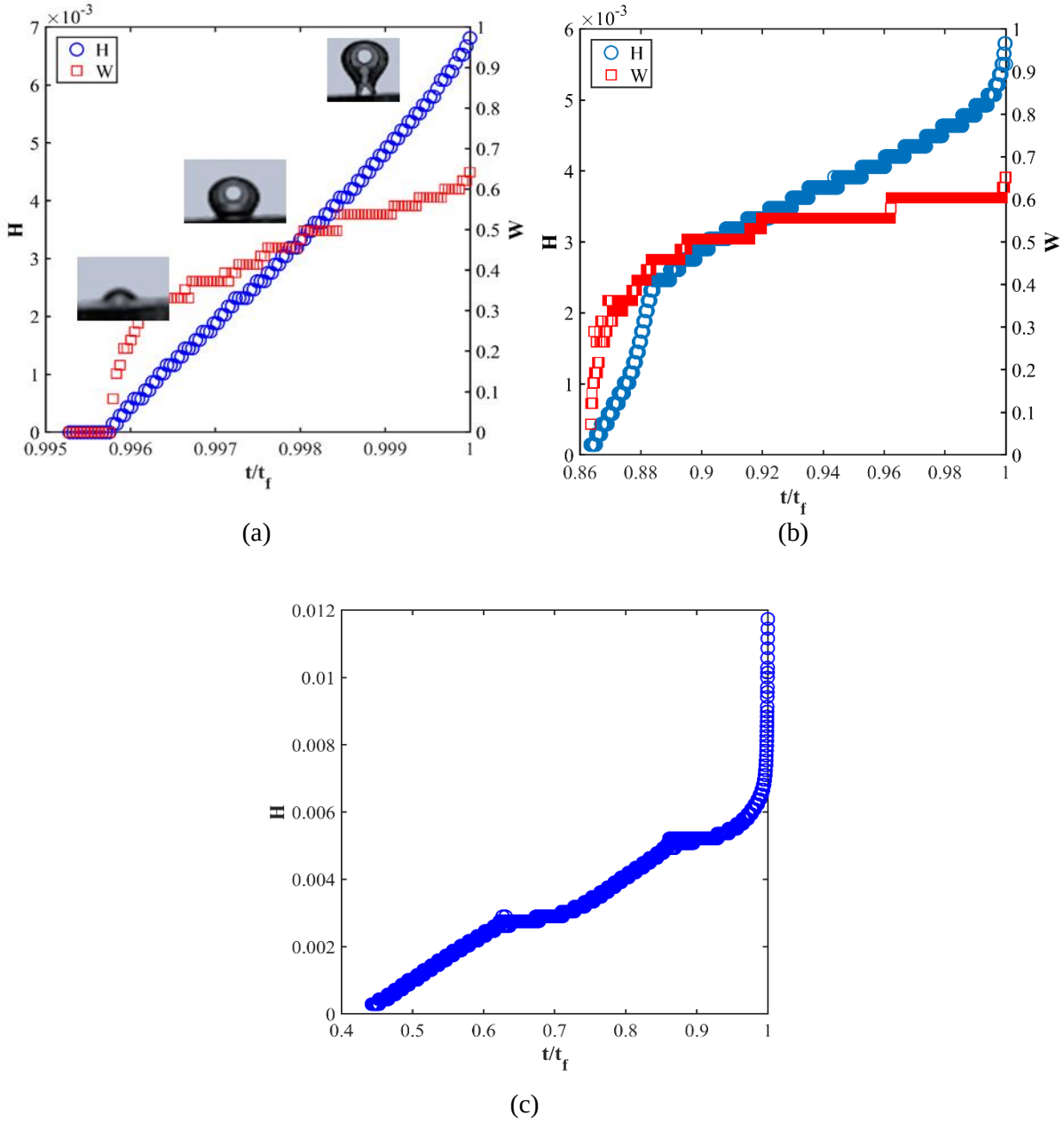

Fig. 9. Variation of the bubble height (H) and maximum with (W) during normalized time in orifices with different surface contact angle a) neutral aluminum b) hydrophilic c) Superhydrophobic

Figure 10 illustrates the overall progression of the bubble center of mass through three distinct stages: weeping, expansion, and detachment. The graph depicts a continuous rise in the height of the bubble center of mass over time. This elevation is attributed to the upward forces accelerating at a greater pace than the downward forces, thereby facilitating an amplified growth rate during the expansion and subsequent detachment of the bubble. The normalized bubble center of mass, denoted as Y/Y_f, signifies the ratio of the current height of the center of mass to the height at which the bubble's center of mass detaches.

Figure 9a & b and Fig. 10a & b unequivocally demonstrate that the superhydrophobic orifice exhibits the greatest height and maximum width during bubble growth, whereas the hydrophilic surface exhibits the lowest measurements. On the superhydrophobic surface, the bubble's height surpasses its width, resulting in the highest center of mass observed. Conversely, on the neutral

aluminum surface, both the maximum width and height of the bubble remain minimal until just before detachment, leading to the lowest center of mass. However, during separation, the height of the bubble on the neutral aluminum surface exceeds that on the hydrophilic surface, amplifying the influence of the bubble's height on the center of mass. Consequently, the center of mass of the bubble on the neutral aluminum surface surpasses that on the hydrophilic surface. In summary, reducing the wettability of the orifice surface augments the height of the bubble's center of mass during separation.

Based on the previous findings, the hydrophilic orifice surface exhibits the smallest bubble volume and height. The hydrostatic downward force $(\rho_l - \rho_g)gz$ exerts a more pronounced effect on the bubble growth time of this surface compared to the other two surfaces. Consequently, the expansion time on the hydrophilic surface is prolonged compared to that on the neutral aluminum surface. Conversely, the superhydrophobic surface, characterized by a high surface tension force, demonstrates the longest expansion time.

The stages of expansion and separation of the bubble can be delineated based on the velocity and acceleration of its center of mass. These stages encompass the elementary stage, middle stage (characterized by almost steady velocity), and final stage (marked by sharp acceleration). Notably, in the neutral aluminum and superhydrophobic orifices, the elementary stage entails retardation acceleration. Conversely, in the hydrophilic orifice, the center of mass of the bubble undergoes accelerative motion during the elementary stage (refer to Fig.10b).

The growth rate of the bubble's center of mass during the expansion stage is highest for the neutral aluminum surface and lowest for the superhydrophobic surface. As the separation moment approaches, the disparity in growth rate between surfaces with different wettability diminishes. Both the normalized volume of the bubble (Fig. 8) and the height of the center of mass (Fig. 10b) indicate that the growth velocity of the bubble is minimal on the superhydrophobic surface during the initial and middle stages, while it reaches its peak on the neutral aluminum surface. However, during the detachment stage, the velocity and acceleration of bubble growth are highest on the superhydrophobic surface and lowest on the hydrophilic surface.

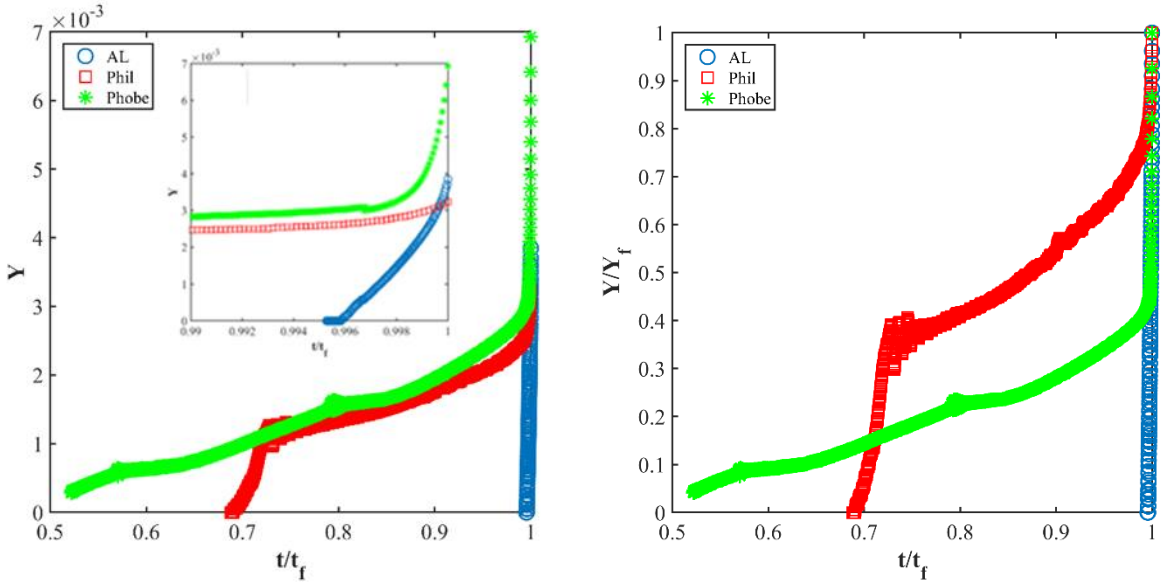

(a) (b)

Fig. 10. Variation of the a) bubble center of mass and b) normalized center of mass during normalized time in orifices with different surface contact angles.

During the initial stage of bubble formation, the surface tension force exerts a considerable influence, primarily because of the small volume of the bubble, rendering the buoyancy force negligible. However, as the bubble volume expands, the buoyancy force gains prominence, resulting in a decrease in the contact angle until it reaches its minimum value. Upon surpassing a certain threshold, the buoyancy force initiates an upward stretching of the bubble, consequently causing the contact angle to rise once more. This upward trend in the contact angle persists until the bubble reaches its separation point.

Figure 11 depicts the evolution of the contact angle of a bubble within orifices featuring a 1 mm diameter under varying surface wettability conditions, with a gas injection flow rate set at 60 mlph. Notably, the contact angles at both the genesis and separation moments of the bubble appear obtuse. On neutral aluminum and hydrophilic surfaces (Fig. 11a), the contact angle of the bubble undergoes significant variation during its growth, with the minimum contact angle reaching an acute value near 40 degrees. Conversely, on the superhydrophobic surface (Fig. 11b), the contact angle of the bubble undergoes minimal change throughout its evolution, remaining obtuse. This observation suggests that the necking time occurs suddenly without the contact angle reaching 90 degrees. Moreover, Fig. 11 highlights that both the initial contact angle at bubble formation and the minimum contact angle during bubble evolution are highest for the superhydrophobic surface, indicating an increase with decreasing orifice surface wettability. However, this increase is comparatively insignificant when comparing the hydrophilic and neutral aluminum surfaces.

Figure 12 presents the correlation between the Reynolds number and various parameters, including flow rate, volume, and center of mass at the moment of bubble separation for orifices with a diameter of 2 mm. From Fig. 12a, it is evident that the Reynolds number of the bubble at separation increases as the volumetric flow rate rises across all surfaces. Furthermore, a decrease in surface wettability corresponds to higher Reynolds numbers, as depicted in Fig.12a. Figure 12b illustrates that lower surface wettability results in a larger detachment volume for the same Reynolds number. This trend is further supported by Fig. 13c, which demonstrates an increase in volume, velocity, and acceleration during the detachment

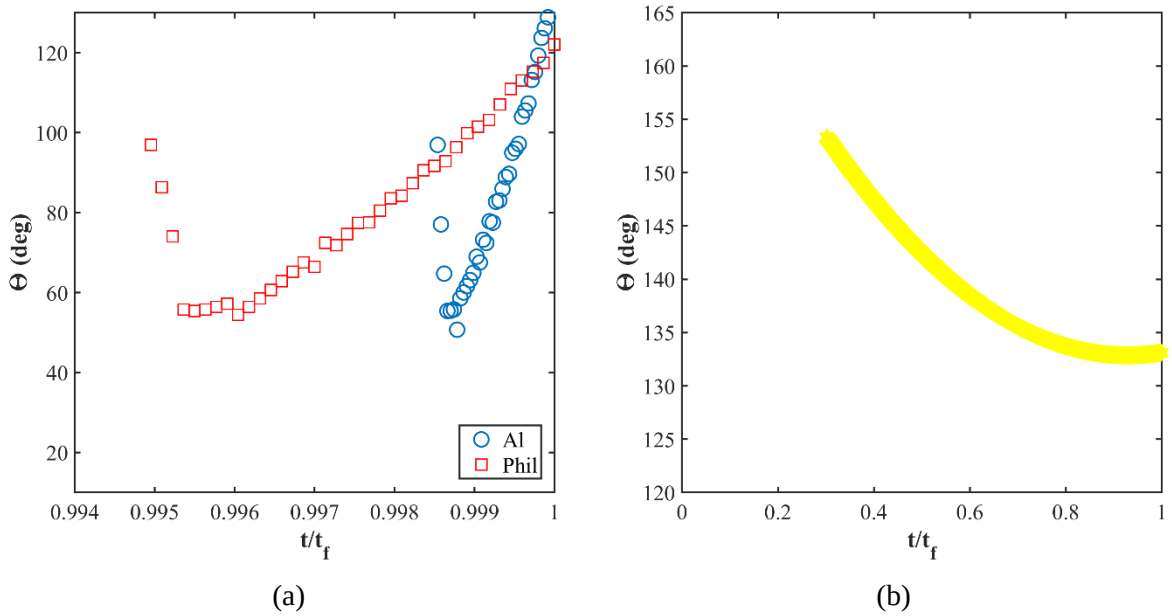

Fig. 11. The variation of the contact angle of the bubble within orifices featuring a 1 mm diameter and different surface contact angles. The gas injection flow rate is maintained at 60 mlph. In (a), the contact angles for neutral aluminum and hydrophilic surfaces are compared, while (b) illustrates the behavior on a superhydrophobic surface.

phase due to decreased surface wettability. Notably, Fig.12c highlights significant differences in the velocity of the bubble at the separation between the superhydrophobic surface and the neutral aluminum and hydrophilic surfaces. This discrepancy is attributed to the higher inertial and drag forces experienced by bubbles in the hydrophobic orifice, driven by the elevated Reynolds numbers and detachment volumes in this scenario.

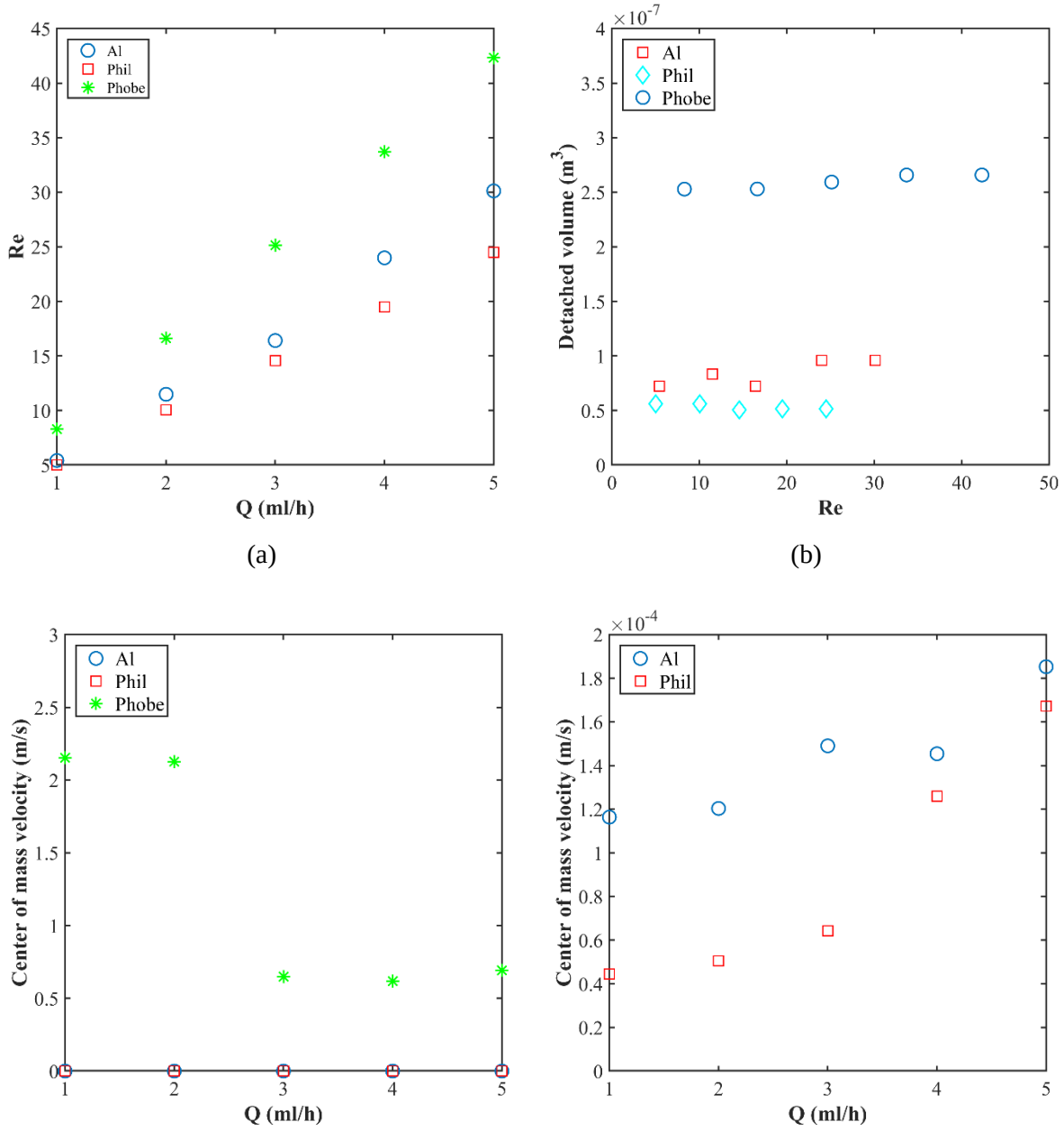

Fig. 12. Variation in a) Reynolds number to the flow rate b) the volume to the Reynolds number c) the center of mass to the flow rate in the detachment moment of the bubble in orifices with different contact angle of surfaces and diameter 2 mm

Figure 13 depicts the forces acting on a growing bubble with an inner diameter of 1 mm and a flow rate of 48 ml/h. We can observe that the momentum force is negligible during the bubble's growth. Additionally, due to the small initial volume of the bubble, the buoyancy force can be disregarded. The increase in bubble volume is primarily caused by the pressure force, which is approximately equal to the surface tension force at the initial stage of growth.

Figure 13a & b illustrate bubble separation on neutral aluminum and hydrophilic surfaces. At this moment, buoyancy and surface tension dominate, while drag and pressure forces are negligible (assuming a quasi-static state). The combined upward force from buoyancy, pressure, and surface tension counterbalances the total force (ΣF), which is always zero. However, the difference between buoyancy and surface tension is relatively small.

Over time, bubble volume and contact area with the surface increase. Buoyancy and surface tension forces rise, while pressure force diminishes. This indicates a shrinking difference between the surrounding hydrostatic pressure $((\rho_l - \rho_g)gz)$ and the pressure difference across the bubble tip $(2\gamma_{lg}/R_0)$. Notably, this reduction is more pronounced for neutral aluminum compared to the hydrophilic surface.

The explanation for this difference lies in the larger volume and contact line changes experienced by the bubble on the neutral aluminum surface during its growth. This larger change amplifies the increase in buoyancy and surface tension forces compared to the hydrophilic case.

Figure 13c reveals a distinct behavior on the superhydrophobic surface. During bubble formation, the surface tension force is significantly larger compared to the neutral aluminum and hydrophilic cases. This amplified surface tension translates to a greater buoyancy force and, consequently, a higher internal pressure within the bubble as it evolves. In contrast to the other surfaces, the pressure force in the superhydrophobic orifice interestingly increases during bubble growth. This observation suggests a growing difference between the surrounding hydrostatic pressure and the pressure difference across the bubble tip. This phenomenon can be attributed to the unique properties of the superhydrophobic surface. The minimal contact area between the bubble and the surface minimizes energy dissipation, potentially leading to a more pronounced pressure build-up within the bubble as it expands. This analysis highlights the significant impact of surface wettability on bubble growth dynamics. Superhydrophobic surfaces can create a scenario where the pressure difference across the bubble tip becomes more prominent compared to the other forces at play.

The analysis of Fig. 13c reveals additional complexities on the superhydrophobic surface. Compared to the other surfaces, the drag force appears to be more significant and exhibits greater variation during bubble expansion. This could be due to the specific texture or roughness of the superhydrophobic surface, which might create additional friction as the bubble grows. Furthermore, during bubble detachment, a noticeable decrease in the drag force vector is observed, indicating an increase in its absolute value. This could be explained by a sudden change in the bubble's interaction with the surface as it pinches off (necking) and detaches. Interestingly, Fig. 13c suggests that as the bubble separates from the superhydrophobic orifice, the forces of buoyancy, surface tension, and pressure experience a rapid increase. This surge in forces might be linked to a rapid change in the bubble shape and surface area during detachment, leading to a rise in the Reynolds number (Re). A higher Re could indicate a more turbulent flow regime around the detaching bubble.

In superhydrophobic surfaces, the surface tension force is the most significant factor, resulting in the highest increase in buoyancy and pressure forces as the bubble volume increases. Unlike hydrophilic and neutral aluminum orifices, the forces in superhydrophobic orifices remain relatively constant until the necking stage. During the necking stage, the hydrostatic pressure force and $2\gamma_{lg}/R_0$ increase in a positive direction at the tip of the bubble, while in neutral aluminum orifices and hydrophilic orifices, the pressure force initially decreases when the bubble appears.

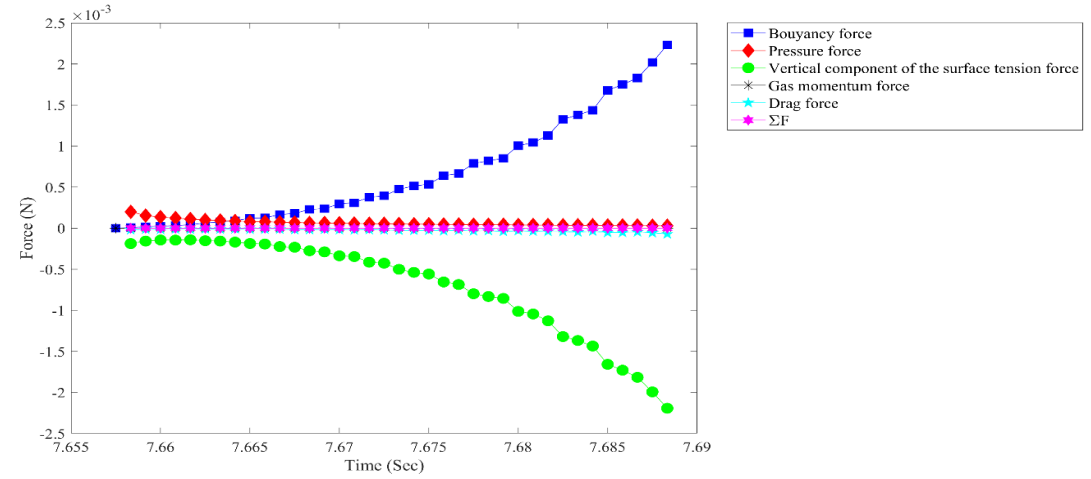

(a)

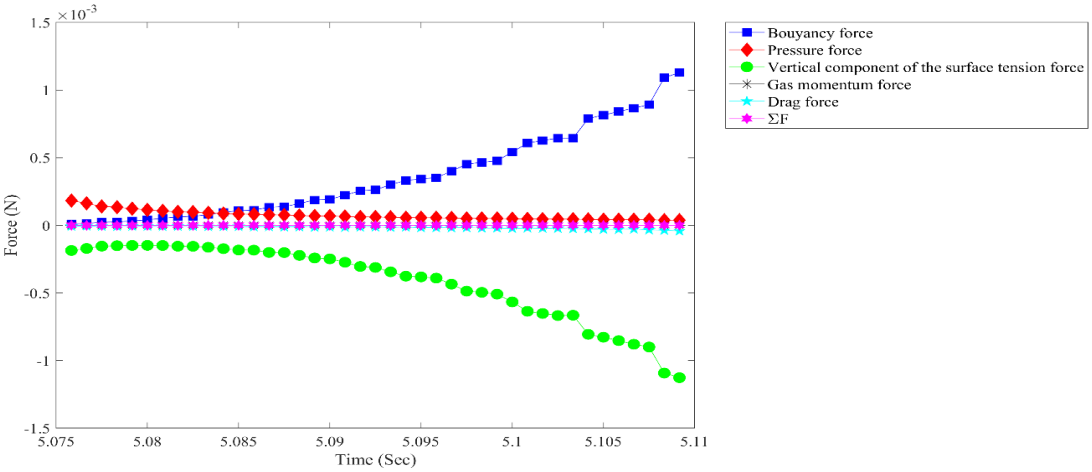

(b)

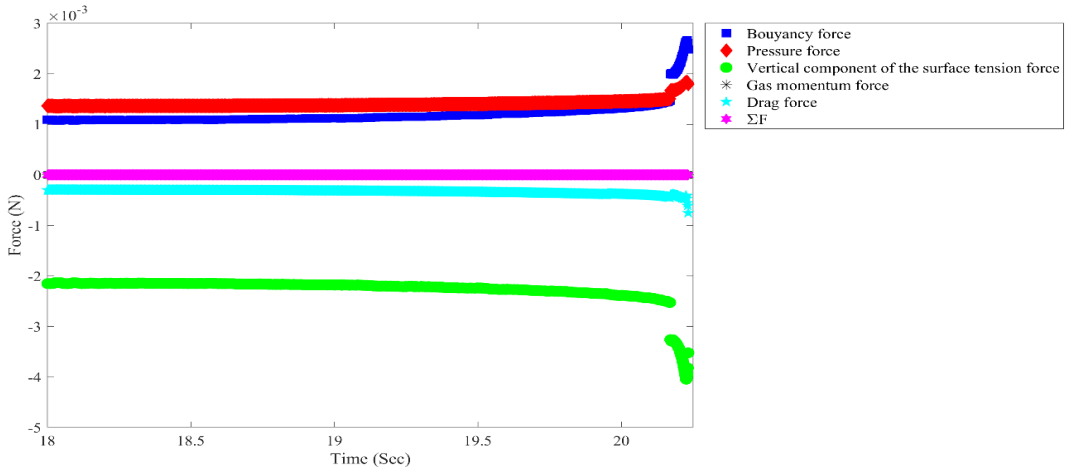

(c)

Fig. 13. Acting forces on a growing bubble from orifices of a) neutral aluminum b) hydrophilic c) superhydrophobic with 1mm diameter in 48mlph flow rate

Separating a bubble from the orifice surface requires overcoming the downward force of surface tension. This is achieved when the combined upward forces, namely buoyancy and pressure, become greater than the surface tension force. This imbalance results in an increase in the momentum force, which acts to propel the bubble upwards. As the momentum force intensifies, the bubble's center of mass experiences an upward acceleration during separation. This acceleration further increases as the upward forces (buoyancy and pressure) become even more dominant. Figure 14 illustrates this concept. It likely presents a bar chart where the x-axis represents the three different orifice wettability conditions (neutral aluminum, hydrophilic, and superhydrophobic) and the y-axis shows the ratio of each individual force acting on a detaching bubble (buoyancy, pressure, surface tension, and momentum) to the total force (sum of all forces). The diameter of the orifice and the flow rate (1 mm and 48 ml/h, respectively) are provided for context.

The rationale behind the observed trends in bubble height and volume variation across different surfaces is elucidated in Fig. 14. In Fig.14 a, it is evident that the neutral aluminum orifice exhibits the highest contribution of buoyancy force during

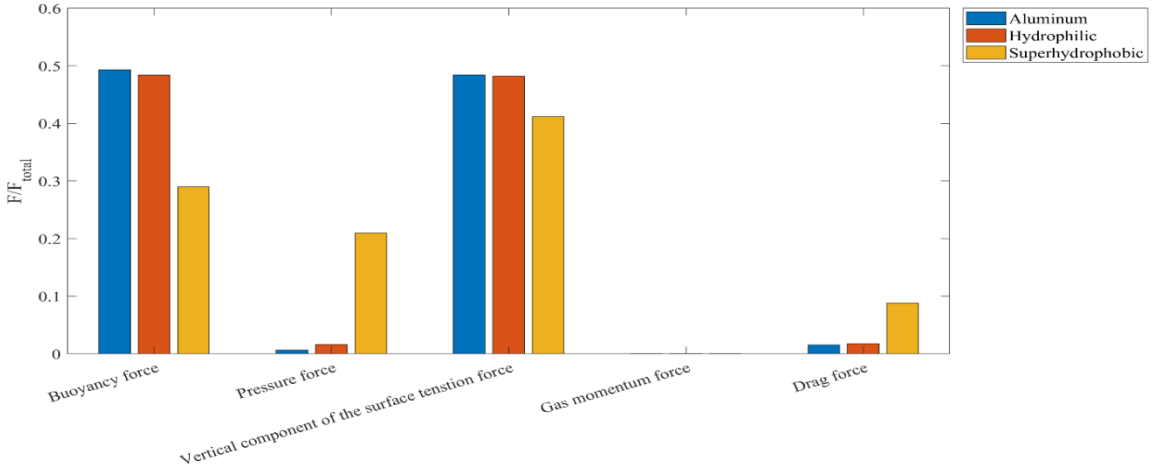

(a)

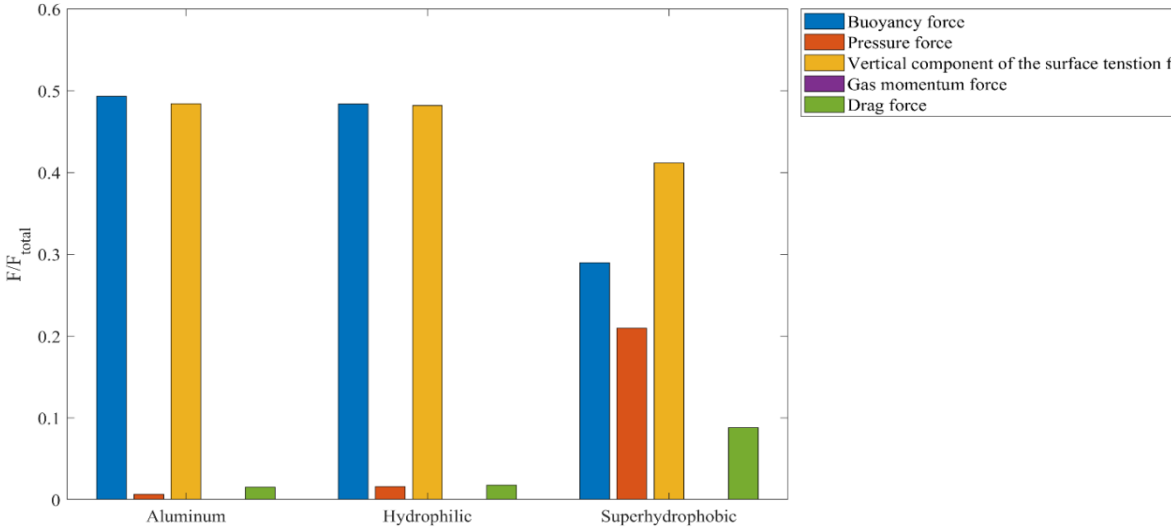

(b)

Fig. 14. The distribution of acting forces on a bubble at the detachment moment from various orifice surfaces. These conditions entail a 1mm diameter orifice and a flow rate of 48mlph.

detachment, whereas the superhydrophobic surface displays the lowest contribution. This trend extends to the surface tension force as well. Notably, the superhydrophobic surface experiences an exceptionally high surface tension force during bubble growth, necessitating a robust upward force such as buoyancy to counteract it effectively. Conversely, the surface tension force exerted on the hydrophilic surface is comparatively minimal, resulting in lower upward force requirements and reduced detachment time. Consequently, this leads to a reduction in bubble volume and a diminished sum of upward and downward forces compared to the superhydrophobic surface (Fig. 14 b).

The superhydrophobic orifice demonstrates the highest proportion of pressure force and drag force, whereas the hydrophilic orifice exhibits the greatest contribution from surface tension force and buoyancy force. Conversely, the neutral aluminum surface displays the highest buoyancy force and the lowest pressure force among all surfaces, leading to accelerated bubble expansion and prolonged weeping time. In contrast, the superhydrophobic surface manifests a notably elevated proportion of drag force and pressure force, which are influenced by the Reynolds number.

4. Conclusion

This study investigated bubble generation from orifices with varying diameters and wettabilities. Airflow rates were injected into submerged orifices, and high-speed photography with image processing analyzed bubble characteristics. Orifice diameter and flow rate significantly impacted bubble volume and formation frequency (inverse proportion). Higher flow rates led to faster formation, while reduced wettability increased formation time (negligible in superhydrophobic case).

Superhydrophobic surfaces exhibited distinct behavior: constant contact line, lower surface tension, and diminished effect of diameter on volume growth. The impact of flow rates became relevant primarily for the superhydrophobic case. Additionally, these surfaces displayed the slowest expansion rate, shortest weeping time, and consistently obtuse contact angles. Drag force was most significant for the superhydrophobic orifice.

These findings highlight the influence of surface wettability on bubble behavior, particularly on superhydrophobic surfaces. Future research could explore additional parameters and develop models for predicting bubble characteristics.

Funding Declaration

There is no funding to declare.

Data Availability

Data sets generated during the current study are available from the corresponding author on reasonable request.

Competing Interest

There is no competing interest to declare.

References

[1] Zimmerman WB, Zandi M, Bandulasena HCH, Tesař V, Gilmour DJ, Ying K. Design of an airlift loop bioreactor and pilot scales studies with fluidic oscillator induced microbubbles for growth of a microalgae Dunaliella salina. Appl Energy. 2011;88(10):3357–69.

[2] Li HY, Lou J, Shang Z, Tang H. Simulation of Bubbly Flow in a Vertical Pipe Using Discrete Phase Model. 2013;1–9.

[3] Li P, Zheng Y, Ran H, Tan J, Lin Y, Zhang Q, et al. Ultrasound triggered drug release from 10-hydroxycamptothecin-loaded phospholipid microbubbles for targeted tumor therapy in mice. Journal of controlled release. 2012;162(2):349–54.

[4] Walters JK, Davidson JF. The initial motion of a gas bubble formed in an inviscid liquid Part 1. The two-dimensional bubble. J Fluid Mech. 1962;12(3):408–16.

[5] Bari S Di, Robinson AJ. Experimental study of gas injected bubble growth from submerged orifices. Exp Therm Fluid Sci. 2013;44:124–37.

[6] Kasimsetty SK, Subramani A, Manglik RM, Jog MA. Theoretical modeling and experimental measurements of single bubble dynamics from a submerged orifice in a liquid pool. In: ASME/JSME 2007 Thermal Engineering Heat Transfer Summer Conference collocated with the ASME 2007

InterPACK Conference. American Society of Mechanical Engineers; 2007. p. 9–17.
[7] Gnyloskurenko S V, Byakova A V, Raychenko OI, Nakamura T. Influence of wetting conditions on bubble formation at orifice in an inviscid liquid. Transformation of bubble shape and size. Colloids Surf A Physicochem Eng Asp. 2003;218(1–3):73–87.
[8] Marmur A, Rubin E. A theoretical model for bubble formation at an orifice submerged in an inviscid liquid. Chem Eng Sci. 1976;31(6):453–63.
[9] Gnyloskurenko S V, Nakamura T, Waseda Y. Review of processes for metallic foams and a basic study of bubble formation in liquids. In: Second International Conference on Processing Materials for Properties. 2000. p. 49–52.
[10] Kasimsetty SK, Subramani A, Manglik RM, Jog MA. Theoretical modeling and experimental measurements of single bubble dynamics from a submerged orifice in a liquid pool. In: ASME/JSME 2007 Thermal Engineering Heat Transfer Summer Conference collocated with the ASME 2007 InterPACK Conference. American Society of Mechanical Engineers; 2007. p. 9–17.
[11] Cai X, Wörner M, Marschall H, Deutschmann O. Numerical study on the wettability dependent interaction of a rising bubble with a periodic open cellular structure. Catal Today. 2016;273:151–60.
[12] Abbassi W, Besbes S, El Hajem M, Ben Aissia H, Champagne JY, Jay J. Influence of operating conditions and liquid phase viscosity with volume of fluid method on bubble formation process. European Journal of Mechanics, B/Fluids. 2017;65:284–98.
[13] Feng X, Kunugi T, Qin S, Wu D. Flowrate effects on the lateral coalescence of two growing bubbles. Can J Chem Eng [Internet]. 2023 Dec 1 [cited 2024 Feb 13];101(12):7263–74. Available from: https://onlinelibrary.wiley.com/doi/full/10.1002/cjce.24976
[14] Vaishnavi GNVS, Ramarajan J, Jayavel S. Numerical studies of bubble formation dynamics in gas-liquid interaction using Volume of Fluid (VOF) method. Thermal Science and Engineering Progress. 2023 Mar 1;39:101718.
[15] Duy TN, Nguyen VT, Park WG. Numerical investigation on influences of injection flow rate on bubbling flow at submerged orifices. European Journal of Mechanics - B/Fluids. 2022 Sep 1;95:23–37.
[16] Reinke P, Ahlrichs J, Beckmann T, Schmidt M. Bubble Dynamics in a Narrow Gap Flow under the Influence of Pressure Gradient and Shear Flow. Fluids 2020, Vol 5, Page 208 [Internet]. 2020 Nov 16 [cited 2024 Feb 13];5(4):208. Available from: https://www.mdpi.com/2311-5521/5/4/208/htm
[17] Sales JMA, Seybold HJ, Oliveira CLN, Andrade JS. Bubble Dynamics in Stationary Two-phase Flow Through Disordered Porous Media. Front Phys. 2022 Mar 21;10:860190.
[18] Corchero G, Montañés JL, Corchero Téllez J. Effect of flow rate conditions on bubble formation. Int J Heat Mass Transf. 2012;55(19–20):5044–52.
[19] Vafaei S, Wen D. Bubble formation on a submerged micronozzle. J Colloid Interface Sci. 2010 Mar;343(1):291–7.
[20] Vafaei S, Angeli P, Wen D. Bubble growth rate from stainless steel substrate and needle nozzles. Colloids Surf A Physicochem Eng Asp. 2011;384(1–3):240–7.
[21] Gerlach D, Biswas G, Durst F, Kolobaric V. Quasi-static bubble formation on submerged orifices. Int J Heat Mass Transf. 2005 Jan;48(2):425–38.
[22] Das AK, Das PK, Saha P. Formation of bubbles at submerged orifices–Experimental investigation and theoretical prediction. Exp Therm Fluid Sci. 2011;35(4):618–27.
[23] Islam MT, Ganesan PB, Sahu JN, Sandaran SC. Effect of orifice size and bond number on bubble formation characteristics: A CFD study. Can J Chem Eng. 2015;93(10):1869–79.
[24] Abbassi W, Besbes S, El Hajem M, Ben Aissia H, Champagne JY, Jay J. Influence of operating conditions and liquid phase viscosity with volume of fluid method on bubble formation process. European Journal of Mechanics, B/Fluids. 2017;65:284–98.
[25] Hanafizadeh P, Sattari A, Hosseini-Doost SE, Nouri AG, Ashjaee M. Effect of orifice shape on bubble formation mechanism. Meccanica. 2018;53(10):2461–83.

[26] Lesage FJ, Cotton JS, Robinson AJ. An equation of motion for bubble growth. ECI Int Conf on Boiling Heat Transfer. 2009;(May):3–7.

[27] Oguz HN, Prosperetti A. Dynamics of Bubble-Growth and Detachment from a Needle. J Fluid Mech. 1993;257:111–45.

[28] Keshock EG, Siegel R. Forces acting on bubbles in nucleate boiling under normal and reduced gravity conditions. National Aeronautics and Space Administration. Lewis Research Center, Cleveland; 1964.

[29] Morrison F. Data correlation for drag coefficient for sphere. Michigan Technology University, Houghton, MI. 2013;6(April):1–2.

[30] Salman AD, Verba A. New approximate equations to estimate the drag coefficient of different particles of regular shape. Periodica Polytechnica Chemical Engineering. 1988;32(4):261–8.

[31] Hanafizadeh P, Sattari A, Hosseini-Doost SE, Nouri AG, Ashjaee M. Effect of orifice shape on bubble formation mechanism. Meccanica. 2018;53(10):1–23.

[32] Vafaei S, Wen D. Modification of the Young-Laplace equation and prediction of bubble interface in the presence of nanoparticles. Adv Colloid Interface Sci. 2015;225:1–15.

[33] Kabanov B, Frumkin A. The size of electrolytically generated gas bubbles. Zeitschrift für Physikalische Chemie A. 1933;166:316–7.